Materials Futures

PAPER • **OPEN ACCESS**

Impact of fabrication methods on binder distribution and charge transport in composite cathodes of all-solid-state batteries

To cite this article: Benjamin Emley *et al* 2023 *Mater. Futures* **2** 045102

OPEN ACCESS
IOP Publishing | Songshan Lake Materials Laboratory
Materials Futures
Mater. Futures 2 (2023) 045102 (9pp)
https://doi.org/10.1088/2752-5724/acefe6

Impact of fabrication methods on binder distribution and charge transport in composite cathodes of all-solid-state batteries

Benjamin Emley[1,6], Chaoshan Wu[1,6], Lihong Zhao[1,2], Qing Ai[3], Yanliang Liang[1,2], Zhaoyang Chen[1], Liqun Guo[1], Tanguy Terlier[4], Jun Lou[3], Zheng Fan[5,*] and Yan Yao[1,2,*]

[1] Materials Science and Engineering Program and Texas Center for Superconductivity at the University of Houston, University of Houston, 4726 Calhoun Rd, Houston, TX 77204, United States of America
[2] Department of Electrical and Computer Engineering, University of Houston, 4726 Calhoun Rd, Houston, TX 77204, United States of America
[3] Department of Materials Science and Nano Engineering, Rice University, 6100 Main Street, Houston, TX 77005, United States of America
[4] SIMS Laboratory, Shared Equipment Authority, Rice University, Houston, TX 77005, United States of America
[5] Department of Engineering Technology, University of Houston, Houston, TX 77204, United States of America

E-mail: yyao4@uh.edu and fanzheng@central.uh.edu

Received 16 May 2023, revised 23 July 2023
Accepted for publication 13 August 2023
Published 29 August 2023

Abstract

The manufacturing process of all-solid-state batteries necessitates the use of polymer binders. However, these binders, being ionic insulators by nature, can adversely affect charge transport within composite cathodes, thereby impacting the rate performance of the batteries. In this work, we aim to investigate the impact of fabrication methods, specifically the solvent-free dry process versus the slurry-cast wet process, on binder distribution and charge transport in composite cathodes of solid-state batteries. In the dry process, the binder forms a fibrous network, while the wet process results in binder coverage on the surface of cathode active materials. The difference in microstructure leads to a notable 20-fold increase in ionic conductivity in the dry-processed cathode. Consequently, the cells processed via the dry method exhibit higher capacity retention of 89% and 83% at C/3 and C/2 rates, respectively, in comparison to 68% and 58% for the wet-processed cells at the same rate. These findings provide valuable insights into the influence of fabrication methods on binder distribution and charge transport, contributing to a better understanding of the binder's role in manufacturing of all-solid-state batteries.

Supplementary material for this article is available online

Keywords: solid-state battery, solvent-free dry process, polymer binder, lithium thiophosphate electrolyte

[6] Equal contribution.
[*] Authors to whom any correspondence should be addressed.

1. Introduction

All-solid-state lithium batteries can potentially offer high specific energy, positioning them as a promising candidate for electric vehicle batteries [1–3]. The elimination of flammable liquid electrolytes could also reduce fire hazards, a concern in current lithium-ion batteries used in electric vehicles [4–6]. In all-solid-state batteries, efficient ion transport could be achieved by thoroughly mixing cathode active material and solid electrolyte (SE) powders in a cathode composite with appropriate microstructural design [7–9].

Currently, the large-scale manufacturing of solid-state batteries lacks a widely reported method [10, 11]. Polymer binders are typically employed in the manufacturing process, which can be categorized as either slurry cast wet or solvent-free dry processes [12–14]. The dominant electrode manufacturing technology is wet process which involves using organic solvent to create a slurry of active materials, conductive carbon and a soluble polymer binder [15, 16]. We previously utilized nitrile butadiene rubber (NBR) in fabricating thin SE membrane [17], leveraging NBR's solubility in nonpolar solvents, which is considered less reactive with sensitive sulfide-based SEs.

Wet processing requires additional solvent recovery steps in battery manufacturing [18]. These steps introduce environmental and safety concerns and adds significant costs [19]. Solvent-free dry processing avoids the use of solvents altogether, minimizing environmental impact and reducing manufacturing costs [20–22]. In the dry process, the shearing force makes polytetrafluoroethylene (PTFE) binder into fibrils, which forms a matrix to blend and support electrode powder together resembling a spider web [13, 21, 23]. Although dry processing mitigates the adverse effects of solvents on the ionic conductivity of sulfide-based SEs, achieving a uniform binder distribution in the composite cathode requires better understanding of the polymer fibrillization process [10].

Furthermore, there is currently no comprehensive study on the effect of polymer binders on the effective partial ionic and electronic conductivities in composite cathodes based on SEs. These conductivities play a crucial role in determining the C-rate capability and, ultimately, the cell performance. Janek *et al* recently investigated the correlation between effective partial conductivities, microstructure and solid-state cell performance [24], highlighting the effect of active material fraction and SE particle size in overcoming charge transport limitations in composite cathodes. However, this study did not investigate the impact of polymer binders and carbon additives on charge transport. Therefore, it is imperative to understand the impact of fabrication methods on binder distribution and their influence on charge transport in solid-state composite cathodes processed with binders [11, 25–27].

In this work, we aim to bridge this gap by investigating the distribution of binders in two distinct fabrication methods: dry process and wet process and by examining how these binders affect the effective partial conductivities in solid-state composite cathodes. Carbon additives were added to the composite to imitate real-world conditions. We used Time-of-Flight Secondary Ion Mass Spectrometry (ToF-SIMS) to map the spatial distribution of binders. Our results reveal that the dry-processed composite cathodes exhibited superior rate performance, demonstrating higher capacity retention of 89% and 83% at C/3 and C/2 rates, respectively, in comparison to 68% and 58% for the wet-processed cells at the same rate. Moreover, we successfully demonstrated a stable all-solid-state lithium cell for 200 cycles at C/3 rate.

2. Methods

2.1. Materials

For both the wet and dry processes, single-crystal $LiNi_{0.83}Mn_{0.06}Co_{0.11}O_2$ (NMC) (MSE Supplies, USA) was used as the cathode active material. Li_6PS_5Cl (LPSCl) (d50 = 5 μm, NEI Corp, USA) was used in both the SE and the composite cathode. Vapor grown carbon fiber (VGCF, PR-19-XT-HHT, Applied Sciences, USA) was used as a conductive additive. NBR (JSR, Japan) was used as the binder in wet processes. In contrast, PTFE (Sigma Aldrich, USA) was the polymeric binder in the dry process. Anhydrous toluene and isobutyl isobutyrate were purchased Sigma Aldrich and used directly. All materials were handled within an argon-filled glove box during the preparation of materials before, during, and after coating processes.

2.2. Fabrication of cathodes with wet process

A predetermined amount of NBR binder was dissolved in a 50:50 w/w mixture of anhydrous toluene (Sigma Aldrich, USA) and $\geqslant$98% isobutyl isobutyrate (Sigma Aldrich, USA). Prior to use, both solvents were treated with molecular sieves for 48 h. The NMC, LPSCl, and VGCF powders at a weight ratio of 70:27:3 was hand-milled in an agate mortar and pestle for 30 min to achieve a homogeneous mixture of the solids before adding the solvent. The solvent and dissolved binder were added to the solids, resulting in a dispersion with a solid loading of 65 wt%. The polymer binder accounted for 0.5 wt% of total solids. To create a semi-stable dispersion, the dispersion and seven pieces of zirconia milling media (Φ : 5 *mm*) were sealed inside of a polypropylene mixing cup and milled for 30 min using a SPEX 8000 M high-energy ball miller. The resulting dispersion was tape-cast onto a silicone-coated polyethylene terephthalate support (Tape Casting Warehouse, USA) through a 400 μm gap set with a doctor blade. The tape casting process was carried out at a speed that yielded a sheer rate of $\sim$20 s^{-1}. Subsequently, the coating was left to dry at room temperature for solvent evaporation. A similar technique was used to fabricate SE coatings using LPSCl but with a solid loading of 54 wt% and 5 wt% NBR binder with respect to LPSCl. The method for tape-casting the SE has been described in our previous work.

2.3. Fabrication of cathodes with dry process

Dry composite cathodes were prepared using the same cathode active material, SE, and VGCF powders used in the wet process. The cathode active material, SE, and VGCF powders were hand-milled with an agate mortar and pestle for 15 min or until a homogenous mixture was achieved. Then, 0.5 wt% PTFE powder was added to this solid mixture and hand-milled for an additional 30 min. During the hand-milling process with PTFE, the materials adhered together, forming a unified and malleable mass under shear force. The mass was then transferred from the mortar and pestle and subjected to shear-rolling between two metal plates. This was achieved by repeatedly rolling a metal cylinder over the metal sheets with the mass in between. The composite was flattened into a sheet form using the manual shearing process until the desired thickness was achieved.

2.4. Fabrication of cathodes with dry processes using solvent-treated LPSCl

In a glass vial, 2.0 g of LPSCl powder was soaked in 5 ml of a 50:50 w/w mixture of anhydrous toluene and $\geqslant$98% isobutyl isobutyrate for 30 min and then dried in a vacuum oven to remove the solvent quickly. This material is referred to solvent-treated LPSCl and is used in the same process described above to fabricate cathodes using the dry process.

2.5. Fabrication of electrochemical cells

Circular coupons with a diameter of 12.7 mm were punched from the coatings to fit precisely inside of a polyether-ether-ketone (PEEK) die cell with Ti rods. For electrochemical evaluation of individual coatings, the coatings were uniaxially pressed at room temperature to 375 MPa and assembled in symmetrical configurations: Ti | LPSCl | Ti, Li | LPSCl | Li, and Ti | Cathode Composite | Ti. The Li | LPSCl | Cathode | LPSCl | Li symmetrical cell was formed by pressing the composite cathode and SE coatings individually at 375 MPa. Then, SE coatings were co-pressed on each side of the composite cathode at 375 MPa. Li metal was then added to the surfaces of the SE coatings. The Li | LPSCl | Cathode full cell was prepared using similar thin SE coupons and composite cathode coupons from both the wet and dry processes. After applying a fabrication pressure of 375 MPa, the cathode had a thickness of 60 μm, resulting in an areal capacity of approximately 2.4 mAh cm^{-2} based on a theoretical specific capacity of around 200 mAh g^{-1} for NMC. Symmetrical cells without Li metal were sealed and held together with a stack pressure of 21 MPa, while cells with Li metal were limited to 7 MPa of stack pressure.

To form LPSCl pellets, 130 mg of LPSCl powder was cold-pressed uniaxially within a PEEK die cell at 375 MPa. 7 mg of carbon powder (Timcal C65, USA) was added to each surface of the pellet to improve the contact between the hard ceramic pellet and the Ti rods. The carbon powder was pressed onto the LPSCl surface at 150 MPa. These cells were sealed and held together with 21 MPa of stack pressure.

2.6. Time-of-flight secondary ion mass spectrometry

ToF-SIMS utilizes a pulsed ion beam to ionize chemical species along an array of a surface of interest which enter a vapor phase upon ionization and are identified with a coupled mass analyzer that provides spectrums showing the mass-to-charge ratios ranging from m/z 1 to m/z 10 000 in a single spectrum. Many spectrums are combined while traversing a 2D array to generate a local map of the chemical species identified by the mass analyzer. This technique enables the creation of chemical images of a surface with a resolution below 500 nm, facilitating the spatially resolved visualization of structures and trace chemical residues in complex samples. Additionally, the ions generated by the primary gun and detected by the mass spectrometer likely have various mass-to-charge ratios, representing a collection of fragments derived from the perceived chemical compounds in the sample. Therefore, calibration is required for analyzing uncommon species of interest, including the PTFE and NBR used in this study.

2.7. Ionic conductivity by electrical impedance spectroscopy

Electrical impedance spectroscopy (EIS) measurements were performed using an electrochemical workstation (SP-300, Bio-Logic Co.) with a 7 mV A.C. perturbation voltage in the frequency range of 7 MHz to 1 Hz and a data collection rate of 10 points per decade. EIS spectra were collected at various temperatures to determine the temperature-dependent ionic conductivity of SEs using a Ti | LPSCl | Ti symmetrical cell. The ionic conductivity of the composite cathode was determined with EIS spectra collected from Li | LPSCl | Cathode | LPSCl | Li 5-layer cells.

2.8. Electronic conductivity via DC polarization method

The electronic conductivity of the composite cathodes in a Ti | Cathode | Ti symmetrical cell was evaluated using the DC polarization technique. An electrochemical potentiostat (SP-300, BioLogic) was employed to apply a constant bias across the Ti electrodes, and the resulting current was measured until a steady state was reached or over a defined period of time. Electrically conductive samples exhibited almost instantaneous stabilization. The measured current and voltage were utilized to calculate the electronic resistance according to Ohm's law.

2.9. Electrochemical characterization of full cells

Full cells with a Li | LPSCl | Cathode configuration were subjected to electrochemical characterization. During the first cycle, the cell was charged from an open circuit voltage $\sim$2.2 V to 4.25 V vs. Li^{+}/Li at a rate of 0.240 mA cm^{-2} using an electrochemical potentiostat (SP-300, BioLogic). Subsequently, the cells underwent discharge and charge processes at various current densities, ranging from 0.240 mA cm^{-2} to 1.20 mA cm^{-2} in the voltage range of 2.5–4.25 V. All evaluations were done at a temperature of 60 °C within a climate-controlled oven.

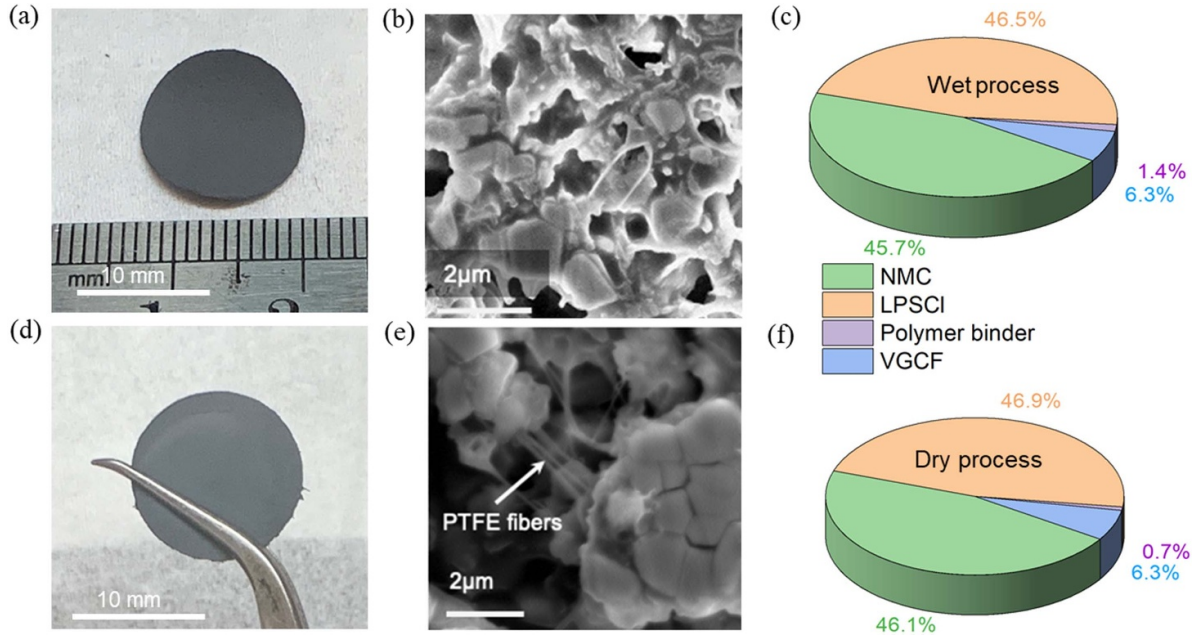

Figure 1. Optical and SEM images showcasing cathode composites obtained through wet and dry processing techniques and their volume fractions. (a)–(c) Wet process; (d)–(f) Dry process.

3. Results and discussions

3.1. Fabrication of composite cathodes using dry and wet processes

A small amount (0.5 wt%) of PTFE and NBR binders were used in the dry and wet processes, respectively, to effectively bind the composite cathodes, creating mechanically robust coatings that were either self-supporting or transferable without any tearing, deformation, or mass loss during handling. Figures 1(a) and (d) show images of a wet-processed and a dry-processed composite cathodes, both having a diameter of 12.7 mm. Irrespective of the binder used, both cathodes exhibit a similar appearance. However, a notable difference arises when examining the binder distribution under a SEM. In the wet process (figure 1(b)), the polymer binder, being soluble in the processing solvent, uniformly coats the surfaces of individual cathode components (e.g., NMC powders, SE powder, VGCF). This uniform coating, however, poses a disadvantage as it acts as both a Li^+ ion and electron insulator, leading to increased tortuosity. On the other hand, during the dry process (figure 1(e)), the PTFE binder forms a fibrillated network that does not fully cover the surface of cathode active materials. This phenomenon has been previously reported and is recognized as beneficial for enhancing charge transport in the composite cathode [8, 28]. SEM images of pristine NMC and LPSCl particles are presented in figure S1. The volume ratio of each component in the composite cathode for the wet and the dry processes is shown in figures 1(c) and (f), respectively.

3.2. Binder distribution analysis through ToF-SIMS mapping

ToF-SIMS was used to analyze the spatial distribution of binders with higher chemical sensitivity [7, 29]. As shown in figure 2(a), ToF-SIMS enables compositional analysis of the distribution of components with spatial resolution using Bi_3^+ cluster as the probe. A field of view of 30 × 30 μm is used for ToF-SIMS imaging. The spectra obtained from the dry-processed cathode (figure 2(b)) revealed the F^- signal (m/z = 19) in the negative mode of ToF-SIMS, serving as the fingerprint for the PTFE binder (figure 2(c)). Similarly, identification of $C_3H_5^+$ fragment (m/z = 41) in the positive mode acted as the fingerprint for locating the NBR polymer binder in the wet-proceed cathode (figures 2(d) and (e)). A detailed description of the techniques for identifying each species of the cathode during the ToF-SIMS analysis can be found in the method section, along with the spectra shown in figures S2(a)–(h) in both positive and negative modes.

In addition to spectral analysis, the chemical distribution is effectively visualized through ToF-SIMS mapping, as depicted in figures 3(a)–(h). Notably, the dry process involving shear rolling exhibits a distinctive fiber-like network of PTFE (figure 3(a)). However, the distribution appears less homogeneous, likely due to the manual shearing process employed in this work. In contrast, the wet process yields a more uniform distribution of the NBR binder (figure 3(e)). Both modes of binder distribution are consistent with the SEM images presented in figure 1.

3.3. Comparison of charge transport in composite cathodes

Previous studies outlined a methodology for determining the effective partial conductivities of composite cathodes [24, 30, 31]. In line with the approach established by Minnmann *et al* [24], we fabricated electron-blocking and ion-blocking cells. To investigate ionic charge transport, ion-conducting and electron-blocking layers of LPSCl SE thin films were attached to both sides of the composite cathode. In contrast to Minnmann *et al* [24], where In/Li electrodes were used,

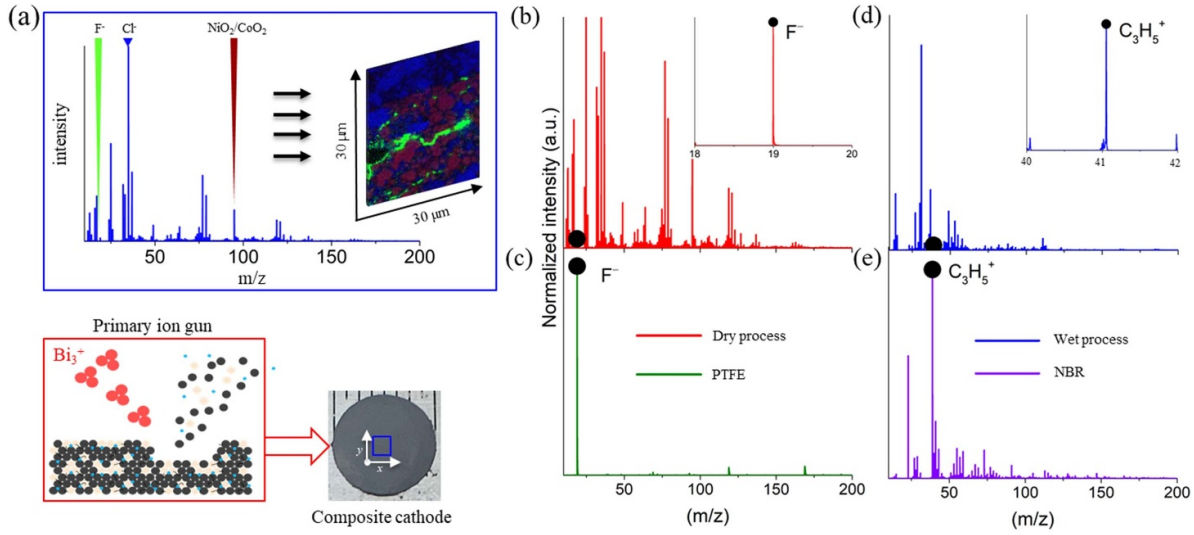

Figure 2. Chemical characterization of a composite cathode using ToF-SIMS. (a) Schematic depicting the working process of ToF-SIMS, along with representative spectra and an image showcasing the chemical information of a composite cathode. (b), (c) SIMS spectra obtained from a dry-processed cathode utilizing a PTFE binder using negative analysis mode. (d), (e) SIMS spectra obtained from a wet-processed sample utilizing a NBR binder using positive analysis mode.

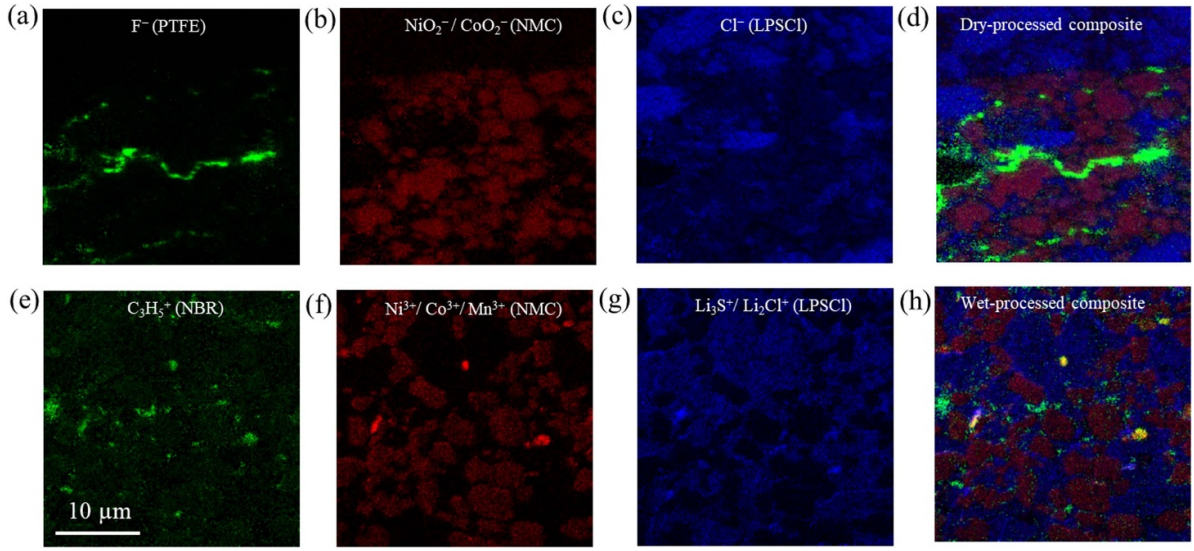

Figure 3. ToF-SIMS mapping of composite cathodes, illustrating the spatial distribution of polymer binders. (a)–(d) Negative-mode ToF-SIMS mapping of a dry-processed sample utilizing a PTFE binder. (e)–(h) Positive-mode ToF-SIMS mapping of a wet-processed sample utilizing a NBR binder.

we opted for lithium metal foils as lithium reservoirs, given the observed stability of the LPSCl–Li interface. EIS test was then conducted to determine the effective conductivity of the composite cathodes.

Figures 4(a) and (b) shows the Nyquist plot and a cross-sectional SEM image of the five-layer cell, with the inset of figure 4(a) presenting the equivalent circuit used for fitting the EIS spectra and a close-up view of the depressed semi-circle at the highest frequency. The full set of EIS spectra at different temperatures ranging from 30 °C to 75 °C is shown in figures S3(a)–(d). These spectra were fitted to a Randles circuit comprising three parallel configurations of resistors and CPEs, representing impedance from the SE, interfaces, and the composite cathode. Notably, the third depressed semi-circle ($\omega \rightarrow 1$ Hz) corresponds to the impedance of the composite cathode.

To gain a deeper understanding of the EIS spectra shown in figure 4(a), a simpler cell configuration, Li|LPSCl|Li, was used. The EIS spectrum of the simplified symmetrical cell reveals two depressed semi-circles in figure S4(b), which emerge within the same frequency range as the first two depressed semi-circles in the 5-layer symmetrical cell

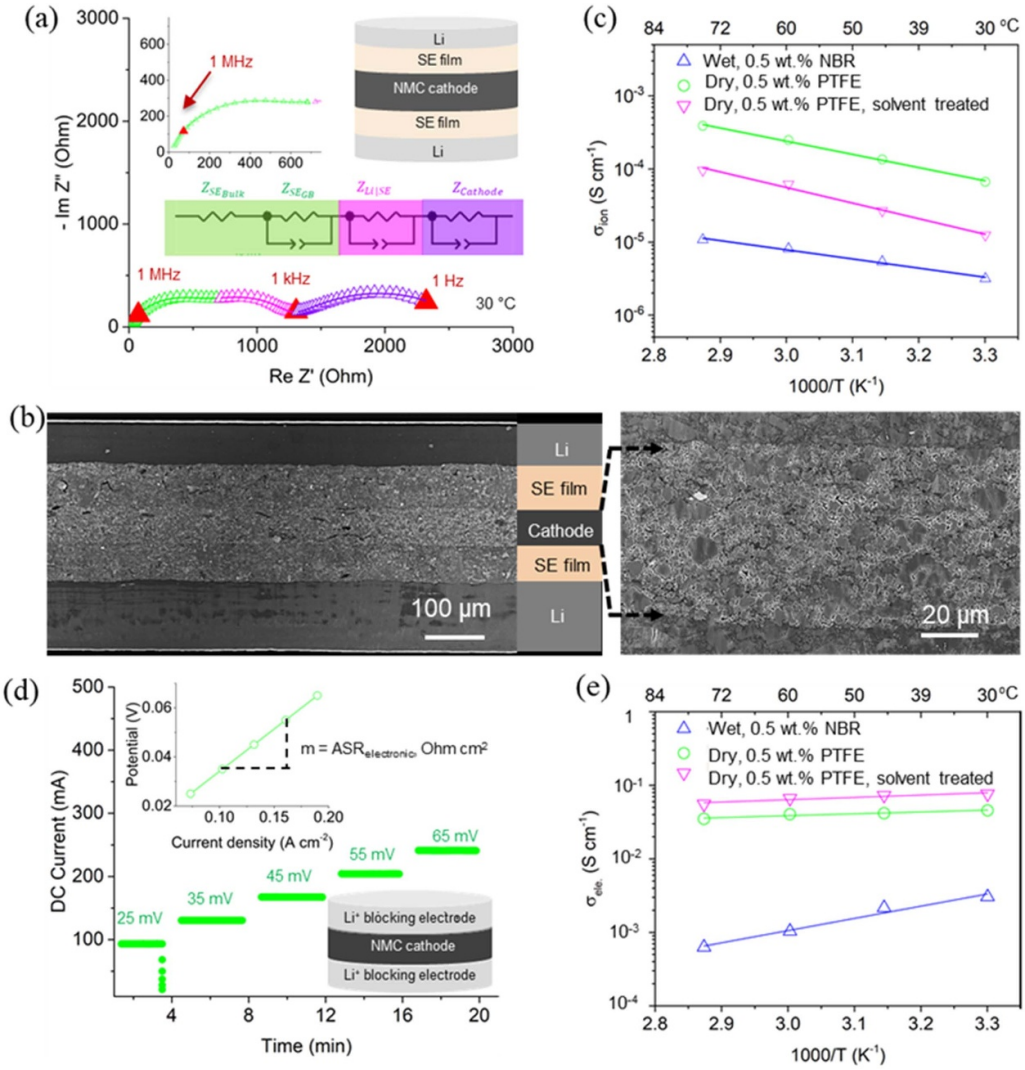

Figure 4. Ionic and electronic conductivity measurement of composite cathodes. (a) Example of EIS using the electron-blocking technique of a composite cathode with insets showing the cell configuration, equivalent circuit model, and close-up of the impedance at high frequency; (b) Cross sectional SEM images of a symmetrical cell with a Li | SE | Cathode Composite | SE | Li configuration; (c) Arrhenius plots for ionic conductivity of the three different composite cathodes; (d) example of the DC polarization technique for a composite cathode at different potentials; (e) Arrhenius plots for electronic conductivity of the three composite cathodes.

shown in figure S4(d). Considering the difference in the number of interfaces and total thicknesses of SE employed in the two symmetrical cells, the amount of resistance scales proportionally.

For investigating electronic charge transport, DC polarization measurements employed electron conducting and lithium-ion blocking titanium electrodes (figure 4(d)). The plots of measured current at various biases and temperatures can be seen in figures S3(e)–(h). Figure 4(d) illustrates that the electronic conductivity dominates over the ionic conductivity, as evident from the immediate flattening and stabilization of the current response to the applied bias during the DC polarization experiment. This behavior is attributed to the presence of 3 wt% VGCF additives in the composite cathodes.

In figure 4(c), the Arrhenius plot of wet and dry-processed composite cathodes showcases distinct behaviors resulting from the processing methods on effective ionic conductivities. Further details is presented in table S1. At 30 °C, the ionic conductivity (σ_{ion}) of dry processed electrode is 6.9×10^{-5} S cm^{-1}, which is 20 times higher than the wet processed counterpart with σ_{ion} of 3.3×10^{-6} S cm^{-1}. In an earlier study when no polymer binder was used in the composite cathodes [24, 30, 32], σ_{ion} of 1.7×10^{-4} S cm^{-1} at the same NMC fraction (70 wt%) was reported. This comparison highlights a substantial 50× reduction in σ_{ion} for the wet-processed electrode, attributable to the ionic-insulating nature of the binder and its uniform coating of binder on the surfaces of individual cathode components. In contrast, the dry process method shows only 2× reduction in σ_{ion}, supporting the observation of the fibrillated network of PTFE binder that does not fully cover the surface of cathode active materials.

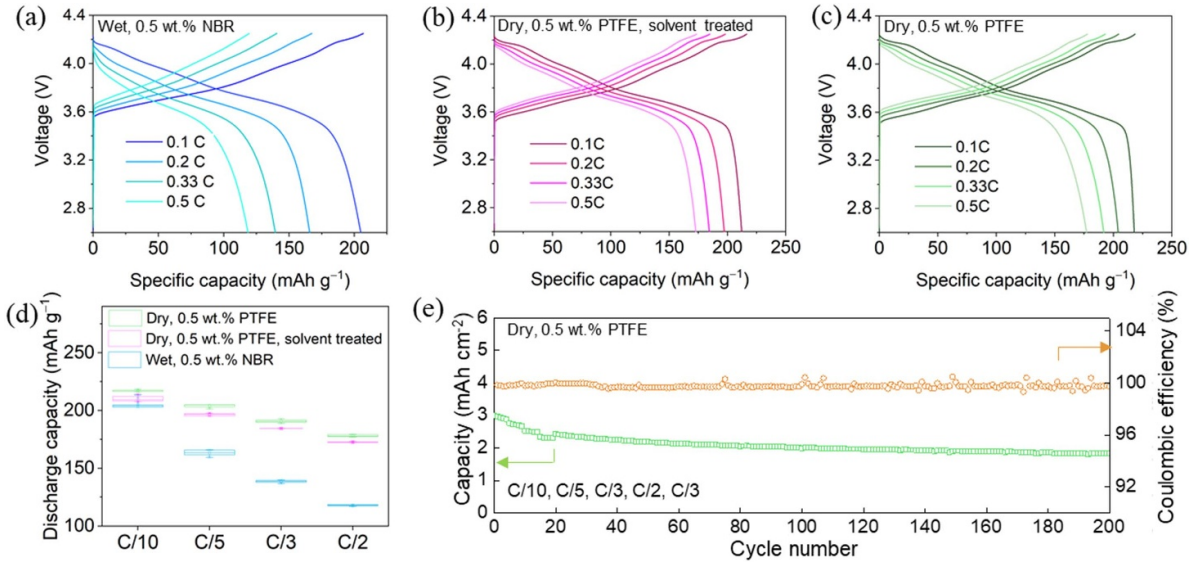

Figure 5. Galvanostatic voltage profiles at various C-rates of full-cell assembled with composite cathodes that were prepared by (a) wet processing, (b) dry-processing but with solvent-treated SE powders, and (c) dry processing using pristine SE powders. (d) The discharge capacities of five cycles at each C-rates. (e) Galvanostatic cycling of the dry-processed cell at C/3 (0.79 mA cm^{-2}). All tests were conducted at 60 °C.

Figure 4(e) illustrates the Arrhenius plot of effective electronic conductivities in wet and dry processed composite cathodes. At 30 °C, the wet process shows an electronic conductivity (σ_{el}) of 3.0 × 10^{-3} S cm^{-1}, which is 15 times lower than the electrodes prepared using the dry process with σ_{el} of 4.6 × 10^{-2} S cm^{-1}. In the same earlier study [24, 30, 32], σ_{el} of 5.6 × 10^{-4} S cm^{-1} at the same NMC fraction (70 wt%) was reported. The higher σ_{el} observed in our work is attributed to the presence of the 3 wt% VGCF additive in the composite cathodes. When examining both wet and dry-processed samples with a 70 wt% NMC fraction, it becomes evident that σ_{el} is approximately 3 orders of magnitude higher than σ_{ion}, highlighting the low σ_{ion} acts as the bottleneck for charge transport in the composite cathode.

To investigate the lower conductivities observed in wet-processed cathodes, which were attributed to the combined effects of solvent and binder, we prepared a sample using the dry process but pre-treated the electrolyte powders with solvent to mimic the solvent's influence. At 30 °C, this sample exhibited σ_{ion} of 1.3 × 10^{-5} S cm^{-1}, which is four times higher than that of the wet process but still five times lower than that of the dry process. This finding indicates that both solvent treatment and binder distribution mode play roughly equally important roles in suppressing ion transport. In contrast, σ_{el} remains similar to dry processed cathode within the experimental error, indicating electron transport is less affected by solvent treatment.

3.4. Comparison of rate performance

The rate performance of solid-state cells fabricated with composite cathodes processed through various fabrication methods is depicted in figures 5(a)–(c). LPSCl pellet and Li metal were used as SE and anode, respectively. To ensure a fair comparison, all three cells had the same loading of active materials (14 mg cm^{-2}). The cells were subjected to testing at various C-rates, ranging from C/10 (0.24 mA cm^{-2}) to C/2 (1.2 mA cm^{-2}), within the voltage range of 2.6–4.25 V vs. Li/Li^{+} at 60 °C. For each C-rate, the cells underwent five cycles, and the discharge capacities were averaged and shown in figure 5(d).

Notably, the cells processed via the dry method exhibited higher capacity retention of 89% and 83% at C/3 and C/2 rates, respectively, compared to the capacity at C/10 rate. In contrast, the wet-processed cells only show 68% and 58% retention at the same rate. At a low rate of C/10, the dry-processed cell outperformed the wet-processed cell by only 8%. However, at a higher rate (C/2), the dry-processed cell demonstrated 43% higher capacity. These results align with the differences observed in ionic conductivity within the composite cathodes. Additionally, figure 5(e) presents the dry-processed cathode sustaining 200 cycles at C/3, exhibiting a high-capacity retention of 76% compared to the first cycle at C/3.

4. Conclusion

In conclusion, we investigated the distribution of binders in two fabrication methods: dry process and wet process. Through the use of electron-blocking and ion-blocking cells, we examined the impact of polymer binders on both ionic and electronic partial conductivities in composite cathodes. Our investigations revealed that the low σ_{ion} serves as the bottleneck in the composite cathode. Significantly, the dry-processed cathodes exhibited a remarkable 20× higher σ_{ion}

compared to wet-processed cathodes, resulting in a 43% higher specific capacity at the rate of C/2. We attributed the underperformance of the wet-processed cathodes to the combined effects of solvent and binder distribution mode. Finally, we successfully demonstrate the stable cycling of all-solid-state lithium cells over 200 cycles. These findings shed light on how fabrication methods profoundly influence the crucial role that binders play in the manufacturing of all-solid-state batteries.

5. Future perspectives

Dry process eliminates the need for solvent mixing, coating, and solvent recovery steps involved in the wet process. This substantial reduction in process time and cost is a significant advantage. However, the application of this technology is still in its early stages, especially for all-solid-state batteries. First, new polymer binder materials that can be easily fibrillated should deserve further attention. Currently, PTFE and copolymers are the predominant binders used in the dry process due to their remarkable low surface energy and ease of fibrillation. Nevertheless, the low LUMO level of PTFE leads to side reactions when used as binders in the anode. Hence, there is a need to create new binders that are electrochemically stable with anode materials such as graphite, silicon, and Li metal. Developing binders with high ionic conductivity is also crucial for enhancing the rate performance of ASSBs. Second, fabricating fully dense, freestanding thin SE membranes remains highly challenging. While the dry process has been successfully demonstrated for large-sheet membranes based on sulfide and halide materials with thicknesses of 15–20 μm, these membranes often contain voids with 1%–5% porosity. This porosity limits the critical current density when Li metal is employed as the anode material. Finally, there is a pressing need to advance precision electrode-making equipment to enable the scale-up of roll-to-roll dry processing. For instance, a high-speed mixer can facilitate binder fibrillation, especially at elevated temperatures when the molecular chain of PTFE becomes more pliable. Additionally, the development of a high-speed calendering machine would significantly expedite the adoption of the dry process on a larger scale. With the above challenges solved, we believe the advancement of dry process technology is poised to reshape the manufacturing landscape of solid-state batteries.

Acknowledgments

This work was supported by the U.S. Department of Energy's Office of Energy Efficiency and Renewable Energy (EERE) under the Vehicle Technologies Program under Contact DE-EE0008864. We appreciate Professor Viktor Hadjiev for Raman spectroscopy measurements and interpretation. The ToF-SIMS analyses were carried out with the support provided by the National Science Foundation CBET-1626418. This work was conducted in part using resources of the Shared Equipment Authority at Rice University.

Conflict of interest

Yan Yao and Zheng Fan have an equity interest in Solid Design Instruments LLC. Yan Yao and Yanliang Liang have an equity interest in LiBeyond LLC.

ORCID iD

Yan Yao https://orcid.org/0000-0002-8785-5030

References

[1] Lee Y G *et al* 2020 High-energy long-cycling all-solid-state lithium metal batteries enabled by silver-carbon composite anodes *Nat. Energy* **5** 299–308
[2] Randau S, Weber D A, Kötz O, Koerver R, Braun P, Weber A, Ivers-Tiffée E, Adermann T, Kulisch J and Zeier W G 2020 Benchmarking the performance of all-solid-state lithium batteries *Nat. Energy* **5** 259–70
[3] Hao F, Liang Y, Zhang Y, Chen Z, Zhang J, Ai Q, Guo H, Fan Z, Lou J and Yao Y 2020 High-energy all-solid-state organic–lithium batteries based on ceramic electrolytes *ACS Energy Lett.* **6** 201–7
[4] Nam Y J, Cho S-J, Oh D Y, Lim J-M, Kim S Y, Song J H, Lee Y-G, Lee S-Y and Jung Y S 2015 Bendable and thin sulfide solid electrolyte film: a new electrolyte opportunity for free-standing and stackable high-energy all-solid-state lithium-ion batteries *Nano Lett.* **15** 3317–23
[5] Wu C S *et al* 2021 Current status and future directions of all-solid-state batteries with lithium metal anodes, sulfide electrolytes, and layered transition metal oxide cathodes *Nano Energy* **87** 23
[6] Chen Y, Kang Y, Zhao Y, Wang L, Liu J, Li Y, Liang Z, He X, Li X and Tavajohi N 2021 A review of lithium-ion battery safety concerns: the issues, strategies, and testing standards *J. Energy Chem.* **59** 83–99
[7] Ai Q, Chen Z, Zhang B, Wang F, Zhai T, Liu Y, Zhu Y, Terlier T, Fang Q and Liang Y 2023 High-spatial-resolution quantitative chemomechanical mapping of organic composite cathodes for sulfide-based solid-state batteries *ACS Energy Lett.* **8** 1107–13
[8] Thieme S, Brückner J, Bauer I, Oschatz M, Borchardt L, Althues H and Kaskel S 2013 High capacity micro-mesoporous carbon–sulfur nanocomposite cathodes with enhanced cycling stability prepared by a solvent-free procedure *J. Mater. Chem.* A **1** 9225–34
[9] Walther F, Koerver R, Fuchs T, Ohno S, Sann J, Rohnke M, Zeier W G and Janek J 2019 Visualization of the interfacial decomposition of composite cathodes in argyrodite-based all-solid-state batteries using time-of-flight secondary-ion mass spectrometry *Chem. Mater.* **31** 3745–55
[10] Li Y, Wu Y, Wang Z, Xu J, Ma T, Chen L, Li H and Wu F 2022 Progress in solvent-free dry-film technology for batteries and supercapacitors *Mater. Today Phys.* **55** 92–109
[11] Tan D H, Meng Y S and Jang J 2022 Scaling up high-energy-density sulfidic solid-state batteries: a lab-to-pilot perspective *Joule* **6** 1755–69
[12] Yao W, Chouchane M, Li W, Bai S, Liu Z, Li L, Chen A X, Sayahpour B, Shimizu R and Raghavendran G 2023 A 5 V-class cobalt-free battery cathode with high loading enabled by dry coating *Energy Environ. Sci.* **16** 1620–30
[13] Ji W, Zhang X, Zheng D, Huang H, Lambert T H and Qu D 2022 Practically accessible all-solid-state batteries enabled by organosulfide cathodes and sulfide electrolytes *Adv. Funct. Mater.* **32** 2202919

[14] Hawley W B and Li J 2019 Electrode manufacturing for lithium-ion batteries—analysis of current and next generation processing *J. Energy Storage* **25** 100862
[15] Sen S, Trevisanello E, Niemöller E, Shi B-X, Simon F J and Richter F H 2021 The role of polymers in lithium solid-state batteries with inorganic solid electrolytes *J. Mater. Chem.* A **9** 18701–32
[16] Sedlmeier C, Kutsch T, Schuster R, Hartmann L, Bublitz R, Tominac M, Bohn M and Gasteiger H A 2022 From powder to sheets: a comparative electrolyte study for slurry-based processed solid electrolyte/binder-sheets as separators in all-solid-state batteries *J. Electrochem. Soc.* **169** 070508
[17] Emley B, Liang Y, Chen R, Wu C, Pan M, Fan Z and Yao Y 2021 On the quality of tape-cast thin films of sulfide electrolytes for solid-state batteries *Mater. Today Phys.* **18** 100397
[18] Lu Y, Zhao C-Z, Yuan H, Hu J-K, Huang J-Q and Zhang Q 2022 Dry electrode technology, the rising star in solid-state battery industrialization *Matter* **5** 876–98
[19] Schnell J, Knörzer H, Imbsweiler A J and Reinhart G 2020 Solid versus Liquid—a bottom-up calculation model to analyze the manufacturing cost of future high-energy batteries *Energy Technol.* **8** 1901237
[20] Al-Shroofy M, Zhang Q, Xu J, Chen T, Kaur A P and Cheng Y-T 2017 Solvent-free dry powder coating process for low-cost manufacturing of $LiNi_{1/3}Mn_{1/3}Co_{1/3}O_2$ cathodes in lithium-ion batteries *J. Power Sources* **352** 187–93
[21] Hippauf F, Schumm B, Doerfler S, Althues H, Fujiki S, Shiratsuchi T, Tsujimura T, Aihara Y and Kaskel S 2019 Overcoming binder limitations of sheet-type solid-state cathodes using a solvent-free dry-film approach *Energy Storage Mater.* **21** 390–8
[22] Ludwig B, Zheng Z, Shou W, Wang Y and Pan H 2016 Solvent-free manufacturing of electrodes for lithium-ion batteries *Sci. Rep.* **6** 23150
[23] Gao S, Su Y, Bao L, Li N, Chen L, Zheng Y, Tian J, Li J, Chen S and Wu F 2015 High-performance $LiFePO_4$/C electrode with polytetrafluoroethylene as an aqueous-based binder *J. Power Sources* **298** 292–8
[24] Minnmann P, Quillman L, Burkhardt S, Richter F H and Janek J 2021 Quantifying the impact of charge transport bottlenecks in composite cathodes of all-solid-state batteries *J. Electrochem. Soc.* **168** 040537
[25] Xiao J, Shi F, Glossmann T, Burnett C and Liu Z 2023 From laboratory innovations to materials manufacturing for lithium-based batteries *Nat. Energy* **8** 1–11
[26] Xu L, Lu Y, Zhao C Z, Yuan H, Zhu G L, Hou L P, Zhang Q and Huang J Q 2021 Toward the scale-up of solid-state lithium metal batteries: the gaps between lab-level cells and practical large-format batteries *Adv. Energy Mater.* **11** 2002360
[27] Hu J-K, Yuan H, Yang S-J, Lu Y, Sun S, Liu J, Liao Y-L, Li S, Zhao C-Z and Huang J-Q 2022 Dry electrode technology for scalable and flexible high-energy sulfur cathodes in all-solid-state lithium-sulfur batteries *J. Energy Chem.* **71** 612–8
[28] Verdier N, Foran G, Lepage D, Prébé A, Aymé-Perrot D and Dollé M 2021 Challenges in solvent-free methods for manufacturing electrodes and electrolytes for lithium-based batteries *Polymers* **13** 323
[29] Zhang J, Chen Z, Ai Q, Terlier T, Hao F, Liang Y, Guo H, Lou J and Yao Y 2021 Microstructure engineering of solid-state composite cathode via solvent-assisted processing *Joule* **5** 1845–59
[30] Kaiser N, Spannenberger S, Schmitt M, Cronau M, Kato Y and Roling B 2018 Ion transport limitations in all-solid-state lithium battery electrodes containing a sulfide-based electrolyte *J. Power Sources* **396** 175–81
[31] Oh D Y, Nam Y J, Park K H, Jung S H, Kim K T, Ha A R and Jung Y S 2019 Slurry-fabricable Li+-conductive polymeric binders for practical all-solid-state lithium-ion batteries enabled by solvate ionic liquids *Adv. Energy Mater.* **9** 1802927
[32] Siroma Z, Sato T, Takeuchi T, Nagai R, Ota A and Ioroi T 2016 AC impedance analysis of ionic and electronic conductivities in electrode mixture layers for an all-solid-state lithium-ion battery *J. Power Sources* **316** 215–23